

# Angular distributions of elastic scattering of $\Sigma^-$ hyperons from nuclei and the $\Sigma$ -nucleus potentials

Toru Harada<sup>1,2,\*</sup> and Yoshiharu Hirabayashi<sup>3</sup>

<sup>1</sup>*Research Center for Physics and Mathematics,  
Osaka Electro-Communication University,*

*Neyagawa, Osaka, 572-8530, Japan*

<sup>2</sup>*J-PARC Branch, KEK Theory Center,*

*Institute of Particle and Nuclear Studies,*

*High Energy Accelerator Research Organization (KEK),*

*203-1, Shirakata, Tokai, Ibaraki, 319-1106, Japan*

<sup>3</sup>*Information Initiative Center, Hokkaido University, Sapporo, 060-0811, Japan*

(Dated: August 13, 2018)

## Abstract

We theoretically investigate the elastic scattering of 50-MeV  $\Sigma^-$  hyperons from  $^{28}\text{Si}$  and  $^{208}\text{Pb}$  in order to clarify the radial distribution of  $\Sigma$ -nucleus (optical) potentials. The angular distributions of differential cross sections are calculated using several potentials that can explain experimental data of the  $\Sigma^-$  atomic X-ray and  $(\pi^-, K^+)$  reaction spectra simultaneously. The magnitude and oscillation pattern of the angular distributions are understood by the use of nearside/farside decompositions of their scattering amplitudes. It is shown that the resultant angular distributions provide a clue to discriminating among the radial distributions of the potentials that have a repulsion inside the nuclear surface and an attraction outside the nucleus with a sizable absorption.

PACS numbers: 21.80.+a, 24.10.Ht, 27.30.+t, 27.80.+w

---

\*Electronic address: harada@isc.osakac.ac.jp

## I. INTRODUCTION

One of the fundamental subjects in hypernuclear study is to understand the properties of hyperon-nucleus interactions. Thus it has been discussed that a study of a negatively charged  $\Sigma^-$  hyperon in nuclear medium would provide valuable information concerning the maximal mass of neutron stars, in which a baryon fraction is found to depend on properties of hypernuclear potentials for neutron stars in astrophysics [1–4].

The systematic study of the  $\Sigma$ -nucleus (optical) potential based on the  $\Sigma^-$  atomic X-ray data was performed by Batty and his collaborators [5–7]. The latest analyses of the  $\Sigma^-$  atomic X-ray have suggested that the  $\Sigma$ -nucleus potential has a repulsion inside the nuclear surface and a shallow attraction outside the nucleus with a sizable absorption [6, 8–11]. Noumi and his collaborators [12, 13] have performed measurements of  $\Sigma$ -hypernuclei by inclusive  $(\pi^-, K^+)$  reactions on C, Si, Ni, In and Bi targets at  $p_\pi=1.20$  GeV/c in KEK-E438 experiments. Their analyses of the  $\Sigma^-$  quasi-free (QF) spectra with a distorted-wave impulse approximation found that the  $\Sigma$ -nucleus potentials have a strong repulsion in the real part and a sizable absorption in the imaginary part within a Woods-Saxon (WS) form:

$$U_\Sigma(r) = (V_0^\Sigma + iW_0^\Sigma)/[1 + \exp((r - R)/a)], \quad (1)$$

where  $(V_0^\Sigma, W_0^\Sigma)=(+90 \text{ MeV}, -40 \text{ MeV})$  with  $R = 1.1A_{\text{core}}^{1/3}$  and  $a = 0.67 \text{ fm}$  [13].

In previous papers [14, 15], we have succeeded to explain simultaneously the data of the  $\Sigma^-$  atoms and the  $(\pi^-, K^+)$  reactions on  $^{28}\text{Si}$  and  $^{208}\text{Bi}$ , using the  $\Sigma$ -nucleus potentials that have a repulsion inside the nuclear surface and an attraction outside the nucleus with a sizable absorption. This repulsion originates from the  $\Sigma N T = 3/2, {}^3S_1$  channel [16–18], whose state corresponds to a quark Pauli-forbidden state in the baryon-baryon system [19–21], and it is a candidate for the appearance of quark degrees of freedom in nuclear physics. Theoretical analyses of the  $(\pi^-, K^+)$  reaction [14, 15] distinguish partially among properties of the  $\Sigma$ -nucleus potential that can reproduce the  $\Sigma^-$  atomic X-ray data sufficiently, whereas the radial distribution of the  $\Sigma$ -nucleus potential inside the nucleus and its strength at the center are hardly determined by fits to the  $\Sigma^-$  QF spectrum. Moreover, we have recognized that an energy dependence of  $(d\sigma/d\Omega)^{\text{opt}}$  in elementary  $\pi^- + p \rightarrow K^+ + \Sigma^-$  processes in nuclei is needed to explain the behavior of the  $(\pi^-, K^+)$  spectrum [14]. Even if using near-recoilless  $(K^-, \pi^+)$  reactions, the radial distribution of the  $\Sigma$ -nucleus potential cannot clearly be determined for a suitable nuclear target such as  $^{58}\text{Ni}$  [22].

Recently, Miwa and his collaborators [23] have proposed an experiment to measure scattering cross sections with high statistics in  $\Sigma^\mp p$  elastic and  $\Sigma^- p \rightarrow \Lambda n$  inelastic scatterings by 500-MeV/c  $\Sigma^\mp$  beam at J-PARC. The purpose of this experiment is to test baryon-baryon interactions based on the flavor SU(3) symmetry and to directly confirm the existence of the quark Pauli-forbidden state in baryon-baryon systems [19, 20].

In this paper, we theoretically investigate the elastic scattering of  $\Sigma^-$  hyperons from nuclei in order to clarify the radial distribution of the  $\Sigma$ -nucleus (optical) potential. We calculate the angular distributions of the differential cross sections in the elastic scattering of  $\Sigma^-$  hyperons from  $^{28}\text{Si}$  and  $^{208}\text{Pb}$  at  $E_{\text{lab}} = 50$  MeV, and demonstrate the sensitivity of the angular distribution to the radial distribution of several potentials that have explained the  $\Sigma^-$  atomic X-ray data and the  $(\pi^-, K^+)$  spectra. It is well-known that optical potential models can describe the elastic scattering of protons or light ions from nuclei, employing appropriate potential parameters phenomenologically. The angular distribution provides specific tests of the validity of the optical potential, in comparison with the experimental data [24]. This is a standard and promising approach for examining the radial distribution of the optical potential in nuclear physics, whereas some ambiguities may still be remained with their strong absorption. Therefore, we believe to examine the radial distribution of the  $\Sigma$ -nucleus potentials with the elastic scattering of  $\Sigma^-$  hyperons from nuclei.

## II. $\Sigma$ -NUCLEUS POTENTIALS

Several theoretical attempts have been performed to construct a  $\Sigma$ -nucleus potential, fitting systematically to strong-interaction shifts and widths of  $\Sigma^-$  atomic X-ray data [6, 7] and manifesting inclusive  $K^+$  spectra in the  $(\pi^-, K^+)$  reaction on nuclear targets [12–15, 25]. The recent status of understanding of the  $\Sigma$ -nucleus potential has been reviewed in Ref. [26]. Here we briefly mention the  $\Sigma$ -nucleus potentials for  $^{28}\text{Si}$  and  $^{208}\text{Pb}$  that we used in this article. The detailed discussion on properties of the potentials are shown in Refs.[14, 15, 22].

In previous papers [14, 15], we have presented several types of the  $\Sigma$ -nucleus potential obtained by fitting to strong-interaction shifts and widths of  $\Sigma^-$  atomic X-ray for various nuclei. The  $\Sigma$ -nucleus potentials that we used are (a) the density-dependent (DD) potential [6], (b) the relativistic mean-field (RMF) potential [9], (c) the local-density approximation

potential (LDA-NF) based on YNG-NF interaction [11, 27], (d) the LDA potential (LDA-S3) based on phenomenological two-body  $\Sigma N$  SAP-3 interaction [10], (e) the shallow potential in the WS form (WS-sh) [28], and (f) the  $t_{\text{eff}}\rho$ -type potential ( $t_{\text{eff}}\rho$ ) [6]. In Fig. 1, we display the real and imaginary parts of several  $\Sigma$ -nucleus potentials for  $^{28}\text{Si}$ , of which all reproduce the experimental shifts and widths of the  $\Sigma^-$  atomic  $4f$  and  $5g$  states sufficiently [14]. The potentials for DD, RMF and LDA-NF have a repulsion inside the nuclear surface and an attraction outside the nucleus, which are considerably different from each other in terms of the repulsion at  $r \lesssim R = 3.34$  fm and the attractive pocket outside there; the potentials for LDA-S3, WS-sh and  $t_{\text{eff}}\rho$  have an attraction at the nuclear center. It was shown that the former potentials (a - c) were favored by the analysis of the  $(\pi^-, K^+)$  reaction, rather than the latter ones (d - f), as discussed in Ref. [14]. However, the radial distribution of the potential inside the nucleus and its strength at the center were hardly determined by fits to the  $(\pi^-, K^+)$  spectrum [14].

———— **FIG. 1** ————

It is important to investigate the  $\Sigma$ -nucleus potential for neutron-excess nuclei like  $^{208}\text{Pb}$ , because one expects to obtain valuable information on the isovector component  $U_1^\Sigma$  in the potential, while the  $\Sigma$ -nucleus potential for  $^{28}\text{Si}$  gives us information on the isoscalar component  $U_0^\Sigma$ . In Fig. 2, we display the real and imaginary parts of several  $\Sigma$ -nucleus potentials for  $^{208}\text{Pb}$ , which is determined by fits to the  $\Sigma^-$  atomic X-ray data. The potentials for DD-A', DD-OBE and LDA-NF have a strong repulsion inside the nuclear surface and an attraction outside the nucleus with a sizable absorption [6, 15], and the potentials for LDA-S3 and  $t_{\text{eff}}\rho$  have an attraction at the nuclear center. In a previous paper [15], we have shown that the former potentials fully reproduce the spectrum of the  $^{209}\text{Bi}(\pi^-, K^+)$  reaction, rather than the latter ones. Thus we have concluded that they provide the ability to explain the data of the  $(\pi^-, K^+)$  reactions as well as those of the  $\Sigma^-$  atoms; but it was impossible to discriminate among the radial distributions of the potentials for DD-A', DD-OBE and LDA-NF inside the nucleus, and it was difficult to clearly see the contributions of the isoscalar and isovector components in this analysis [15].

———— **FIG. 2** ————

### III. THEORY

We calculate the differential cross sections by solving the radial part of the non-relativistic Schrödinger equation as a scattering problem:

$$\left[ \frac{\hbar^2}{2\mu} \left( -\frac{d^2}{dr^2} + \frac{L(L+1)}{r^2} \right) + U_\Sigma(r) + U_{\text{Coul}}(r) \right] R_L(r) = ER_L(r), \quad (2)$$

where  $R_L$  is a radial wave function with angular momentum  $L$ ;  $U_\Sigma$  is the  $\Sigma$ -nucleus potential,  $U_{\text{Coul}}$  is the Coulomb potential with a uniform distribution of charge for  $R_C = 1.2A^{1/3}$ ,  $\mu$  is the  $\Sigma^-$  nucleus reduced mass, and  $E = \hbar^2 k^2 / (2\mu)$  is the incident energy of the center-of-mass frame. It is noted that the potentials of  $U_\Sigma$  seem to include effects of a nuclear spin-orbit potential because they can reproduce the data of the  $\Sigma^-$  atomic ( $n\ell$ ) states and ( $\pi^-$ ,  $K^+$ ) reactions. However, as far as the elastic scattering of  $\Sigma^-$  hyperons at the low-energy like  $E_{\text{lab}} = 50$  MeV is concerned, the effects of the spin-orbit potential on the differential cross section are negligible, as we will discuss later.

The angular distribution of the differential cross section in the elastic scattering is written as

$$\sigma_{\text{el}}(\theta) = |f(\theta)|^2 = |f_N(\theta) + f_F(\theta)|^2, \quad (3)$$

where  $f(\theta)$  is the elastic scattering amplitude, which is often decomposed into traveling-waves decomposition of the nearside (N) and farside (F) components,  $f_N(\theta)$  and  $f_F(\theta)$  [29, 30]. They denote the sum of the Coulomb and nuclear parts as

$$f_{\text{N,F}}(\theta) = f_{\text{N,F}}^{(\text{Coul})}(\theta) + f_{\text{N,F}}^{(\text{Nucl})}(\theta) \quad (4)$$

with

$$f_{\text{N,F}}^{(\text{Nucl})}(\theta) = \frac{i}{2k} \sum_L (2L+1) e^{2i\sigma_L^{(\text{C})}} (1 - S_L) \tilde{Q}_L^{(\mp)}(\cos\theta), \quad (5)$$

where  $\sigma_L^{(\text{C})}$  and  $S_L$  are the Coulomb phase shift and the S-matrix element in the elastic scattering, respectively. The traveling-wave function  $\tilde{Q}_L^{(-)}$  ( $\tilde{Q}_L^{(+)}$ ) corresponds to the nearside (farside) component, and it is defined in terms of the Legendre functions [29]:

$$\tilde{Q}_L^{(\pm)}(\cos\theta) = \frac{1}{2} \left[ P_L(\cos\theta) \mp i \frac{2}{\pi} Q_L(\cos\theta) \right]. \quad (6)$$

In the semi-classical limit, they can be associated with trajectories that pass the near side and the far side of the scattering center. Therefore, this decomposition gives a good understanding of the behavior of the angular distribution depending on the nuclear potential that has an attraction and/or a repulsion with a strong absorption [29, 30]. The angular distributions for the nearside and farside contributions denote  $\sigma_N(\theta) = |f_N(\theta)|^2$  and  $\sigma_F(\theta) = |f_F(\theta)|^2$ , respectively. Because the  $\Sigma$ -nucleus potential has a sizable absorption, the angular distribution of  $\Sigma^-$  hyperons from nuclei may behave similar to that of light composite nuclei rather than that of protons.

#### IV. RESULTS AND DISCUSSION

Let us consider the elastic scattering of  $\Sigma^-$  hyperons from  $^{28}\text{Si}$  [9, 31]. We calculate the angular distribution of the differential cross section in this elastic scattering, using several types of the  $\Sigma$ -nucleus potential (see Fig. 1). Here we assume the  $\Sigma^-$  incident energy of  $E_{\text{lab}} = 50$  MeV in the laboratory frame.

In Fig. 3, we show the calculated angular distributions of the cross section  $\sigma_{\text{el}}$  from  $^{28}\text{Si}$ , together with the nearside  $\sigma_N$  and farside  $\sigma_F$  components. It is clearly seen that the angular distributions for DD, RMF and LDA-NF differ from those for LDA-S3, WS-sh and  $t_{\text{eff}}\rho$ . This implies that the potentials of the former are fully distinguishable from those of the latter, and it supports our previous results on the analysis of the  $(\pi^-, K^+)$  reaction [14, 15].

In the angular distributions for DD, RMF and LDA-NF, the diffraction oscillations arise from the Fraunhofer interference between the nearside  $f_N$  and farside  $f_F$  amplitudes, and reach their maximum amplitude at  $\theta \simeq \bar{\theta}$ , where the angle  $\bar{\theta}$  for  $\sigma_N(\bar{\theta}) = \sigma_F(\bar{\theta})$  is called a ‘‘Fraunhofer crossover’’ and hence  $\bar{\theta} = 40^\circ - 50^\circ$  in the cases of these potentials. Forward of the crossover, the farside is dominant, while for angles somewhat larger than  $\bar{\theta}$ , the nearside dominates. This oscillations is damped with increasing  $\theta$  because of the falloff of the farside components  $\sigma_F$ . The dominance of  $\sigma_F$  at small angles is caused by the Coulomb attraction for  $\Sigma^-$  hyperons that have a negative charge, and by the attraction pocket of the  $\Sigma$ -nucleus potentials at the nuclear surface; the dominance of  $\sigma_N$  at large angles is due to the strong repulsive components in the potentials for DD, RMF and LDA-NF. It is very interesting because this situation is completely opposite to that of the normal nucleus-nucleus scattering where  $\sigma_N$  dominates at small angles owing to the Coulomb repulsion, and

$\sigma_F$  becomes dominant with increasing  $\theta$  owing to the strong attraction in nucleus-nucleus potentials [29, 30]. The behavior of the angular distribution in the nucleus-nucleus elastic scattering has been studied in the case of the repulsive nucleus-nucleus potential at high incident energies of  $E/A \gtrsim 300$  MeV [32].

In the cases of the potential for  $t_{\text{eff}}\rho$ , WS-sh and LDA-S3, the slope and oscillation pattern of their angular distributions differ appreciably. For  $t_{\text{eff}}\rho$ , we find that  $\sigma_F$  is dominant over all angles because the  $\Sigma$ -nucleus potential is attractive, in addition to the Coulomb attraction. For LDA-S3, the oscillations are clearly observed owing to the Fraunhofer crossover between  $\sigma_F$  and  $\sigma_N$  at  $\theta \simeq 90^\circ$  and the magnitude of  $\sigma_N$  is something large at  $\theta \gtrsim 90^\circ$  because the real part of the potential is repulsive at  $r \simeq 1.8\text{--}2.6$  fm, as seen in Fig. 1. The situation for WS-sh seems to be on the way from LDA-S3 to  $t_{\text{eff}}\rho$ .

Therefore, we show that the angular distribution of the  $\Sigma^-$  elastic-scattering differential cross section from  $^{28}\text{Si}$  provides a classification for properties of the  $\Sigma$ -nucleus potentials.

———— **FIG. 3** ————

In Fig. 4, we compare the cross sections for DD, RMF and LDA-NF in order to evaluate the detailed discrimination of properties of the potential inside the nucleus. We notice that the magnitudes of their angular distributions ( $\sigma_{\text{el}}$ ) differ appreciably at angles  $\theta \gtrsim 60^\circ$ , where the magnitude and shape of  $\sigma_{\text{el}}$  are affected by the radial distribution of the potential inside the nuclear surface. Indeed, a notch test suggests that the magnitude and shape of  $\sigma_{\text{el}}$  at angles  $\theta \gtrsim 90^\circ$  are sensitive to the radial distribution of the potential at  $r \simeq 2.6$  fm, which corresponds to the region of the inner repulsion of the potential, depending on the strength of the imaginary parts.

———— **FIG. 4** ————

For DD, RMF or LDA-NF, moreover, the attractive pocket of the potential at the nuclear surface with the Coulomb attraction plays an important role in making a diffraction structure of the angular distribution, so that it leads the nearside component to be large, and causes a strong oscillation of the angular distribution. To clarify this effect, we study behavior of the angular distribution  $\sigma_{\text{el}}$  using the WS potential that has only the repulsion in the real part and a sizable absorption in the imaginary part, for example, WS30 defined as  $(V_0^\Sigma, W_0^\Sigma) = (+30 \text{ MeV}, -40 \text{ MeV})$  in Eq. (1). In Fig. 5, we show the calculated angular

distribution for WS30, as compared with that for RMF. We find that the magnitude of  $\sigma_F$  for WS30 falls off rapidly on its steep slope with increasing  $\theta$  from the forward angle. Thus this diffraction oscillations are shifted toward the forward angle and their magnitude becomes small. This is caused by the lack of the attraction at the nuclear surface in the repulsive WS30 potential.

Consequently, it is shown that the angular distribution for the elastic scattering of 50-MeV  $\Sigma^-$  hyperons from  $^{28}\text{Si}$  gives additional information to discriminate among the radial distributions of the potentials inside the nucleus, e.g., inner repulsion and attractive pocket, which were not able to be identified by the analysis of the  $\Sigma^-$  atomic X-ray and  $(\pi^-, K^+)$  reaction. It implies that the elastic scattering of  $\Sigma^-$  hyperons from nuclei is a powerful tool for identifying the radial distribution of the potential by the use of the diffraction pattern influenced by the nuclear repulsion and the Coulomb attraction, rather than  $\Sigma^+$  hyperons acting on the nuclear repulsion with the Coulomb repulsion.

———— **FIG. 5** ————

We consider the elastic scattering of  $\Sigma^-$  hyperons from  $^{208}\text{Pb}$ , which has a large attraction of the Coulomb interaction. We calculate the angular distribution of the differential cross section ( $\sigma_{\text{el}}$ ) at  $E_{\text{lab}} = 50$  MeV, using several types of the  $\Sigma$ -nucleus potential (see Fig. 2). In Fig. 6, we show the calculated angular distributions of  $\sigma_{\text{el}}$ , together with the nearside  $\sigma_N$  and farside  $\sigma_F$  components, respectively.

In the cases of DD-A', DD-OBE and LDA-NF, we find the similar behavior of their results in the angular distribution, where a difference between the  $\Sigma$ -nucleus potentials for  $^{208}\text{Pb}$  is not so enhanced, in comparison with that for  $^{28}\text{Si}$ . This recalls the fact that the effect on the  $\Sigma$ -nucleus potential is rather masked by the strong Coulomb potential in  $^{208}\text{Pb}$ , as discussed in Ref. [22]. However, we recognize that the diffraction pattern in  $^{208}\text{Pb}$  differs from that in  $^{28}\text{Si}$  as follows: As increasing  $\theta$  the former  $\sigma_F$  falls off on a steep slope more rapidly than the latter  $\sigma_F$ , and hence the former  $\sigma_N$  dominates at  $\theta \gtrsim 30^\circ$ . Thus the Fraunhofer crossover is slightly shifted toward the forward angle. Moreover, a lot of Fraunhofer oscillations in  $^{208}\text{Pb}$  appear, which may correspond to the grazing angular momentum  $L_g \simeq 13$  ( $L_g \simeq 6$  in  $^{28}\text{Si}$ ) for LDA-NF if  $L_g$  is defined as a value at the transmission  $T_L = 1/2$  [30]. The oscillation spacing between maxima  $\Delta\theta$  is also reduced in  $^{208}\text{Pb}$ .

In the case of  $t_{\text{eff}}\rho$ , we find that  $\sigma_F$  is dominant in all angles and  $\sigma_N$  is negligible, so that



the oscillations in  $\sigma_{\text{el}}$  are indistinctive. This originates from the fact that both the  $\Sigma$ -nucleus potential and the Coulomb potential are strongly attractive. For LDA-S3, we also find that  $\sigma_{\text{F}}$  is dominant as well as that of  $t_{\text{eff}}\rho$ , but  $\sigma_{\text{N}}$  is not negligible because the potential for LDA-S3 has a weaker attraction than that for  $t_{\text{eff}}\rho$ . The oscillations in  $\sigma_{\text{el}}$  are clearly shown at angles  $\theta > 120^\circ$  by the appearance of the crossover.

———— **FIG. 6** ————

In Fig. 7, we show the angular distributions of the cross sections for DD-A', DD-OBE and LDA-NF in order to evaluate the repulsive components and radial distributions of their potentials inside the nucleus. We compare the results on DD-A' with those on DD-OBE, because the former has the inner repulsion of  $\sim 80$  MeV at the nuclear center and the latter has that of  $\sim 30$  MeV in the similar potential form, depending on the imaginary part of individual potentials. Thus we realize that the magnitudes of their  $\sigma_{\text{el}}$  are sufficiently discriminable at  $\theta \gtrsim 60^\circ$ . Moreover, let us compare the results on LDA-NF with those on DD-OBE, because the radial distributions of their potentials differ markedly whereas the inner repulsions at the nuclear center are almost the same. Thus we can see that the oscillation patterns of their  $\sigma_{\text{el}}$  are slightly different. Consequently, we recognize that the angular distribution of the  $\Sigma^-$  elastic-scattering differential cross section from  $^{208}\text{Pb}$  provides the ability to discriminate among the radial distributions of the potentials inside the nucleus.

———— **FIG. 7** ————

As mentioned in Sect.III, the potentials of  $U_\Sigma$  seem to include the effects of the nuclear spin-orbit potential because they can reproduce the data of the  $\Sigma^-$  atomic ( $n\ell$ ) states and ( $\pi^-$ ,  $K^+$ ) reactions, though our calculations do not deal with the spin-orbit term explicitly. However, it is one of the important subjects to study the spin-orbit potential for a  $\Sigma$  hyperon [16], whereas the experimental information is extremely limited. According to several theoretical predictions [33–36], here, we consider the spin-orbit potential for  $\Sigma$  with the strength of  $V_{\text{so}}^\Sigma \simeq \frac{1}{2}V_{\text{so}}^N$ , where  $V_{\text{so}}^N$  for a nucleon. When we use the potential for RMF including artificially a spin-orbit term of  $V_{\text{so}}^\Sigma(1/r)[df(r)/dr]\boldsymbol{\sigma}\cdot\mathbf{L}$  which is often used, we show that the calculated angular distributions are almost the same as those for the original RMF in the elastic scattering of 50-MeV  $\Sigma^-$  hyperons from  $^{28}\text{Si}$ , e.g.,  $\sigma_{\text{el}}(\theta)$  at the first maximum for  $\theta \simeq 50^\circ$  is increased by only about 6%. This small difference originates from the fact that the

$\Sigma^-$  elastic scattering at  $E_{\text{lab}} = 50$  MeV is regarded as a low-energy one, in comparison with high-energy scatterings of  $E_{\text{lab}} \simeq 100\text{--}300$  MeV, where the spin-orbit effects could fairly act because the contribution of large  $L$ 's to the differential cross section is important. For  $^{208}\text{Pb}$  the situation is the same as that for  $^{28}\text{Si}$ .

## V. CONCLUSION

We have theoretically investigated the elastic scattering of 50-MeV  $\Sigma^-$  hyperons from  $^{28}\text{Si}$  and  $^{208}\text{Pb}$  in order to clarify the radial distribution of the  $\Sigma$ -nucleus potentials. The angular distributions of their differential cross sections have been calculated using several potentials that can explain the experimental data of the  $\Sigma^-$  atomic X-ray and  $(\pi^-, K^+)$  spectra simultaneously. We have discussed the behavior of the magnitude and oscillation pattern in the angular distribution by the use of the nearside/farside decomposition of the elastic scattering amplitude, and we have examined a competition between the attraction of the Coulomb interaction and the repulsion/attraction in the  $\Sigma$ -nucleus potentials. As far as the low-energy elastic scattering like  $E_{\text{lab}} = 50$  MeV is concerned, the effects of the spin-orbit potential on the angular distribution are very small.

In conclusion, the angular distribution of the differential cross sections in the 50-MeV  $\Sigma^-$  elastic scattering from  $^{28}\text{Si}$  and  $^{208}\text{Pb}$  provides additional information to discriminate the nature of the repulsion/attraction inside the nuclear surface in the  $\Sigma$ -nucleus potentials where it was not uniquely determined by the  $\Sigma^-$  atomic X-ray data and the  $(\pi^-, K^+)$  and  $(K^-, \pi^+)$  spectra. We expect that the elastic scattering experiments of  $\Sigma^-$  hyperons from nuclear targets are carried out at J-PARC facilities in the future, in spite of some experimental difficulties. More theoretical investigations of the  $\Sigma^-$  scattering for several incident energies and targets are required.

### Acknowledgments

The authors are obliged to Professor K. Tanida and Dr. K. Miwa for valuable discussion and comments. This work was supported by Grants-in-Aid for Scientific Research (C)

(No. 22540294).

---

- [1] S. Balberg and A. Gal, Nucl. Phys. **A625**, 435 (1997).
- [2] M. Baldo, G.F. Burgio, and H.-J. Schulze, Phys. Rev. C **61**, 055801 (2000).
- [3] T. Takatsuka, Y. Yamamoto, and R. Tamagaki, Int. J. Mod. Phys. B**15**, 1609 (2001).
- [4] J. Schaffner-Bielich, Nucl. Phys. **A835**, 279 (2010).
- [5] C.J. Batty, et al., Phys. Lett. **B74**, 27 (1978).
- [6] C.J. Batty, E. Friedman, and A. Gal, Phys. Lett. **B335**, 273 (1994); C.J. Batty, E. Friedman, and A. Gal, Prog. Theor. Phys. Suppl. **117**, 227 (1994).
- [7] C.J. Batty, E. Friedman, and A. Gal, Phys. Rep. **287**, 385 (1997).
- [8] T. Yamada and Y. Yamamoto, Prog. Theor. Phys. Suppl. **117**, 241 (1994).
- [9] J. Mareš, E. Friedman, A. Gal, and B.K. Jennings, Nucl. Phys. **A594**, 311 (1995).
- [10] T. Harada, *Proceedings of the 23rd INS International Symposium on Nuclear and Particle Physics with Meson Beams in the 1 GeV/c Region*, Tokyo, March, 1995 (Universal Academy Press, Inc., Tokyo, 1995) p. 211.
- [11] J. Dabrowski, J. Rozynek, and G.S. Anagnostatos, Eur. Phys. J. A **14**, 125 (2002).
- [12] H. Noumi, et al., Phys. Rev. Lett. **89**, 072301 (2002); H. Noumi, et al., Phys. Rev. Lett. **90**, 049902(E) (2003).
- [13] P. K. Saha, et al., Phys. Rev. C **70**, 044613 (2004).
- [14] T. Harada and Y. Hirabayashi, Nucl. Phys. **A759**, 143 (2005).
- [15] T. Harada and Y. Hirabayashi, Nucl. Phys. **A767**, 206 (2006).
- [16] C.B. Dover, D.J. Millener, and A. Gal, Phys. Rep. **184**, 1 (1989), and references therein.
- [17] T. Harada, Y. Akaishi, S. Shinmura, and H. Tanaka, Nucl. Phys. **A507**, 715 (1990).
- [18] T. Harada and Y. Akaishi, Phys. Lett. **B262**, 205 (1991).
- [19] M. Oka, K. Shimizu, and K. Yazaki, Nucl. Phys. **A464**, 700 (1987).
- [20] Y. Fujiwara, Y. Suzuki, and C. Nakamoto, Prog. Part. Nucl. Phys. **58**, 439 (2007).
- [21] T. A. Rijken, M. M. Nagels, and Y. Yamamoto, Prog. Theor. Phys. Suppl. **185**, 14 (2010).
- [22] T. Harada and Y. Hirabayashi, Nucl. Phys. **A829**, 100 (2009).
- [23] K. Miwa, et al., *Measurement of the cross sections of  $\Sigma p$  scatterings*, Proposal for Nuclear and Particle Physics Experiments at the J-PARC (2010),

- [http://j-parc.jp/NuclPart/Proposal\\_e.html](http://j-parc.jp/NuclPart/Proposal_e.html).
- [24] B.A. Watson, P.P. Singh, and R.E. Segel, *Phys. Rev.* **182**, 977 (1969); F.D. Becchetti Jr. and G.W. Greenlees, *Phys. Rev.* **182**, 1190 (1969).
  - [25] M. Kohno, Y. Fujiwara, Y. Watanabe, K. Ogata, and M. Kawai, *Prog. Theor. Phys.* **112**, 895 (2004).
  - [26] E. Friedman and A. Gal, *Phys. Rep.* **452**, 89 (2007), and references therein.
  - [27] Y. Yamamoto and H. Bandō, *Prog. Theor. Phys. Suppl.* **81**, 9 (1985).
  - [28] R.S. Hayano, *Nucl. Phys.* **A478**, 113c (1988); M. Iwasaki, doctoral dissertation, University of Tokyo, 1987 (unpublished).
  - [29] R. C. Fuller, *Phys. Rev. C* **12**, 1561 (1975).
  - [30] K.W. McVoy and G.R. Satchler, *Nucl. Phys.* **A417**, 157 (1984).
  - [31] T. Furumoto, Y. Sakuragi, and Y. Yamamoto, *Nucl. Phys.* **A835**, 362 (2010).
  - [32] T. Furumoto, Y. Sakuragi, and Y. Yamamoto, *Phys. Rev. C* **82**, 044612 (2010).
  - [33] O. Morimatsu, S. Ohta, K. Shimizu, K. Yazaki, *Nucl. Phys.* **A420** (1984) 573; Y. Fujiwara, M. Kohno, T. Fujita, C. Nakamoto, Y. Suzuki, *Nucl. Phys.* **A 674**, 493 (2000).
  - [34] C.B. Dover, A. Gal, *Prog. Part. Nucl. Phys.* **12** (1984) 171.
  - [35] J. Mareš and B.K. Jennings, *Phys. Rev. C* **49**, 2472 (1994); J. Mareš and B.K. Jennings, E.D. Cooper, *Prog. Theor. Phys. Suppl.* **117**, 415 (1994).
  - [36] N. Kaiser, *Phys. Rev. C* **71**, 068201 (2005); *Phys. Rev. C* **76**, 068201 (2007).

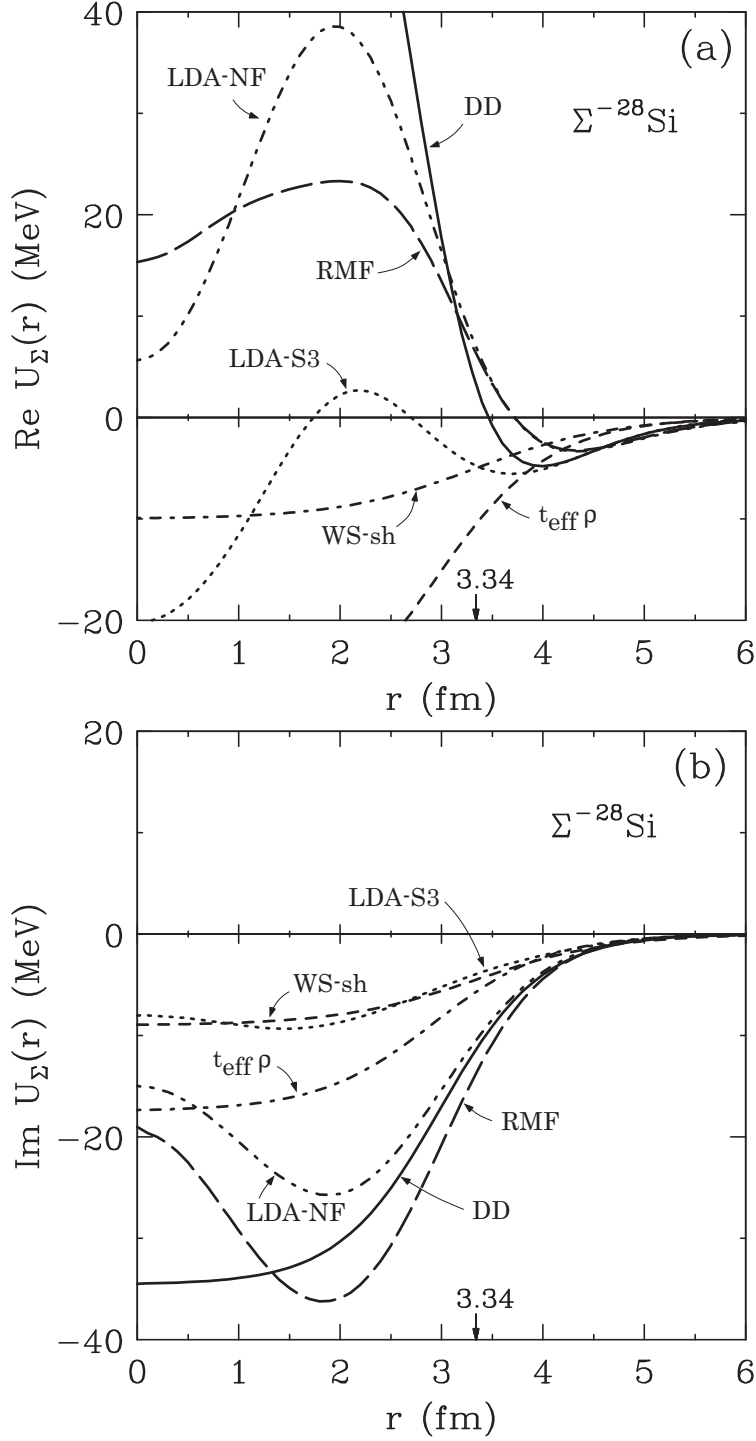


FIG. 1: Real (a) and imaginary (b) parts of the  $\Sigma$ -nucleus potential  $U_\Sigma$  for  $^{28}\text{Si}$ , as a function of the radial distance between the  $\Sigma^-$  and the nucleus  $^{28}\text{Si}$ . The Coulomb potential is not included in the real part of each potential. Curves denote the potentials for DD, RMF, LDA-NF, LDA-S3, WS-sh and  $t_{\text{eff}}\rho$  [14]. The arrows at  $r = 1.1A_{\text{core}}^{1/3} = 3.34$  fm denote the nuclear radius of the  $\Sigma^-$ - $^{28}\text{Si}$  system.

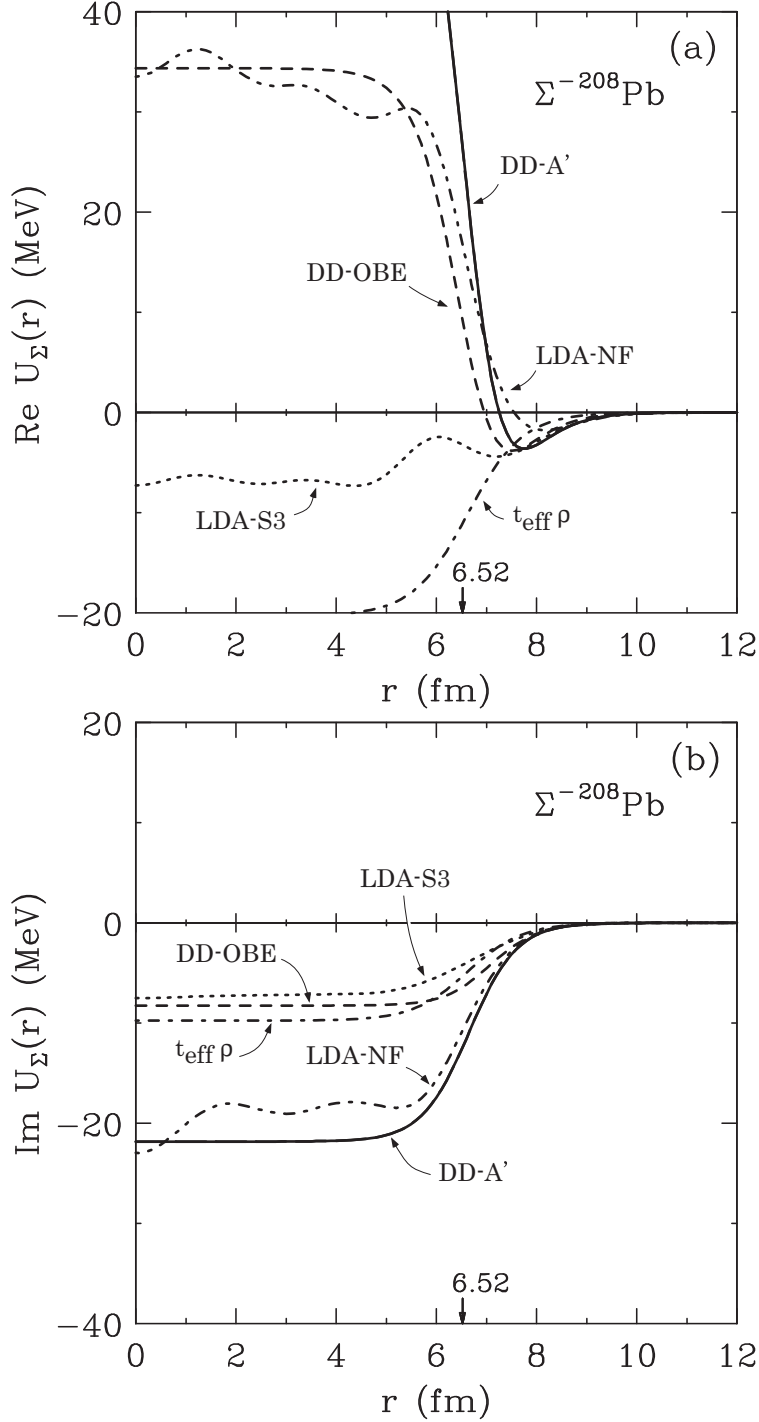


FIG. 2: Real (a) and imaginary (b) parts of the  $\Sigma$ -nucleus potentials  $U_\Sigma$  for  $^{208}\text{Pb}$ , as a function of the radial distance between the  $\Sigma^-$  and the nucleus  $^{208}\text{Pb}$ . The Coulomb potential is not included in the real part of each potential. Curves denote the potentials for DD-A', DD-OBE, LDA-NF, LDA-S3 and  $t_{\text{eff}}\rho$  [15]. The arrows at  $r = 1.1A_{\text{core}}^{1/3} = 6.52$  fm denote the nuclear radius of the  $\Sigma^-$ - $^{208}\text{Pb}$  system.

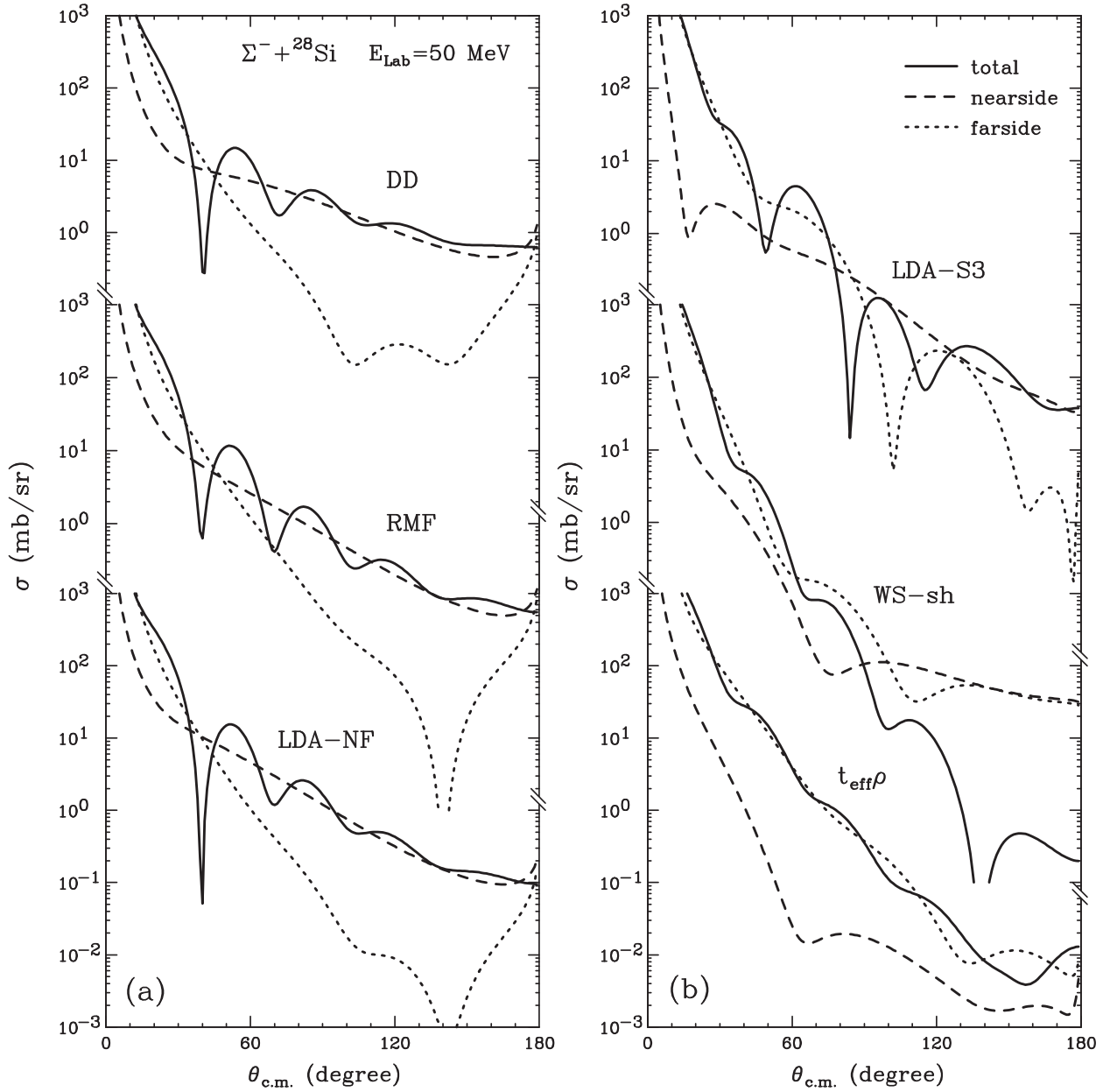


FIG. 3: Calculated angular distributions for the 50-MeV elastic scattering of  $\Sigma^-$  hyperons from  $^{28}\text{Si}$ . Curves draw the absolute values obtained with the  $\Sigma$ - $^{28}\text{Si}$  potentials (a) for DD, RMF and LDA-NF, and (b) for LDA-S3, WS-sh and  $t_{\text{eff}}\rho$ . Solid, dashed and dotted curves denote the values for total, nearside and farside components in the cross sections, respectively.

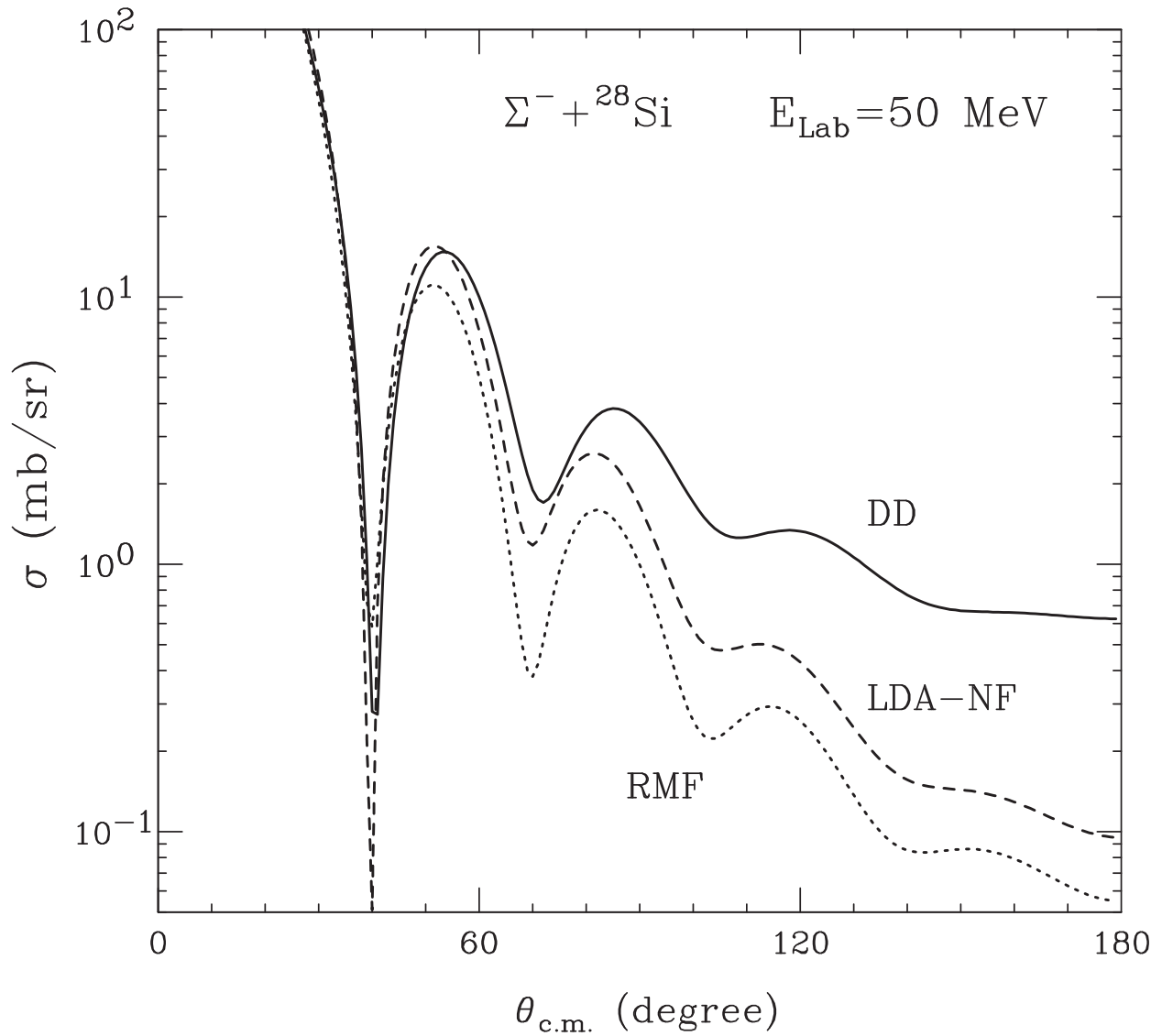


FIG. 4: A comparison with the calculated angular distributions for the 50-MeV  $\Sigma^-$  hyperon elastic scattering from  ${}^{28}\text{Si}$ . Solid, dashed and dotted curves denote the values obtained with the potentials for DD, RMF and LDA-NF in  $\Sigma^-$ - ${}^{28}\text{Si}$  systems, respectively.



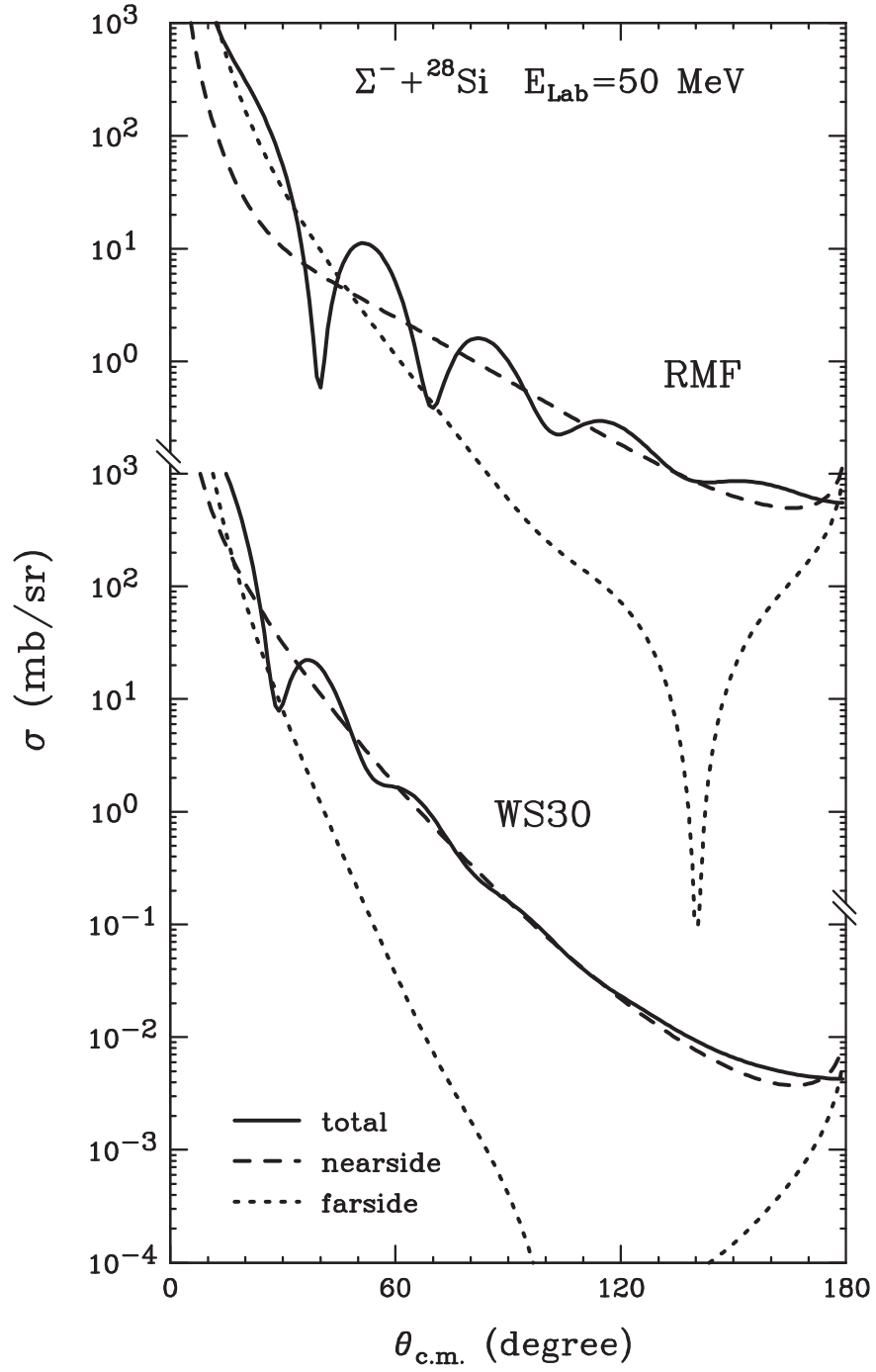


FIG. 5: Calculated angular distributions for the 50-MeV  $\Sigma^-$  hyperon elastic scattering from  ${}^{28}\text{Si}$ , in comparison between RMF and WS30. Solid, dashed and dotted curves denote the values for total, nearside and farside components in the cross sections, respectively.

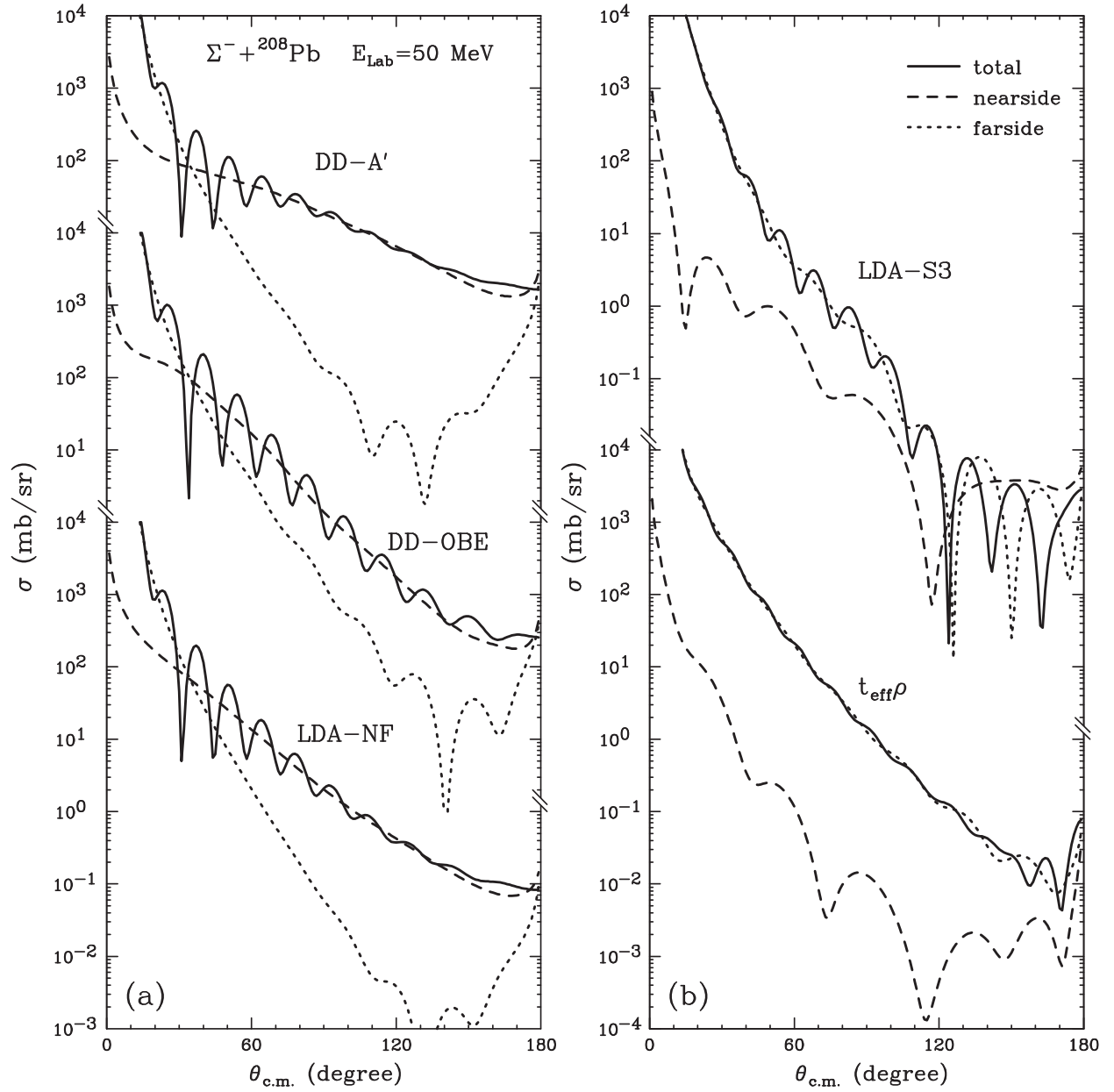


FIG. 6: Calculated angular distributions for the 50-MeV elastic scattering of  $\Sigma^-$  hyperons from  $^{208}\text{Pb}$ . Curves draw the absolute values obtained with the  $\Sigma^-$ - $^{208}\text{Pb}$  potentials (a) for DD-A', DD-OBE and LDA-NF, and (b) for LDA-S3 and  $t_{\text{eff}}\rho$ . See also the caption to Fig. 3.

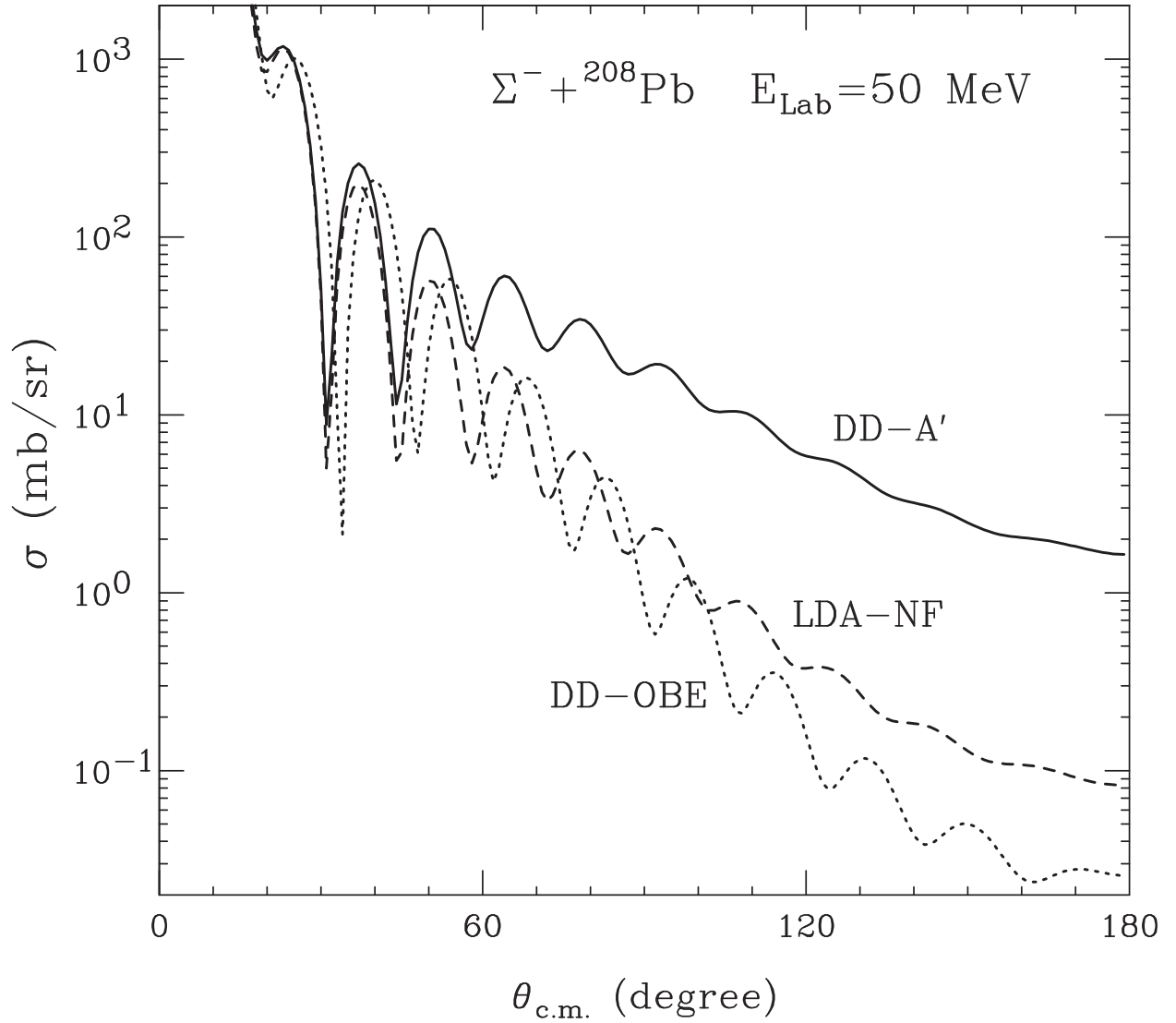


FIG. 7: A comparison with the calculated angular distributions for the 50-MeV  $\Sigma^-$  hyperon elastic scattering from  $^{208}\text{Pb}$ . Solid, dashed and dotted curves denote the values for the potentials for DD-A', LDA-NF and DD-OBE in  $\Sigma^-$ - $^{208}\text{Pb}$  systems, respectively.